Progress in Potential Formation and Radial-Transport-Barrier Production for Turbulence Suppression and Improved Confinement in GAMMA 10

T. Cho, H. Higaki, M. Hirata, H. Hojo, M. Ichimura, K. Ishii, K. Md. Islam, A. Itakura, I. Katanuma, J. Kohagura, R. Minami, Y. Nakashima, T. Numakura, T. Saito, Y. Tatematsu, M. Yoshikawa, O. Watanabe, Y. Kubota, T. Kobayashi, Y. Yamaguchi, Y. Higashizono, Y. Miyata, H. Saimaru, A. Mase[1)], Y. Yasaka[2)], A. Kojima[3)], M. Yoshida[3)], W. Horton[4)], T. Imai, V. P. Pastukhov[5)], S. Miyoshi, and GAMMA 10 Group

Plasma Research Centre, University of Tsukuba, Tsukuba, Ibaraki 305-8577, Japan

e-mail contact of main author: tcho@prc.tsukuba.ac.jp

Abstract. **(1)** A ***transverse energy-transport barrier*** is ***externally controlled*** for the first time by *off-axis electron-cyclotron heating* (ECH). This ***internal energy-transport barrier*** is produced by ECH controlled cylindrical-layer formation ($4<r_c<7$ cm) with energetic electrons. The electrons flow through the whole device and are partially lost into the end region. As a result, a radially localized *ambipolar-potential bump*, with *strongly sheared electric fields* E_r (or peaked vorticity) is formed along with the direction reversal of $\boldsymbol{E}_r\times\boldsymbol{B}$ shear flow near the Φ_C peak. This leads to ***suppress*** *L-mode-like intermittent* ***turbulent vortex-like structures*** *near the layer* in the central cell, and results in $\boldsymbol{T_e}$ **and** $\boldsymbol{T_i}$ **rises** surrounded by this strong shear flow layer *just like* the *characteristics of an internal transport barrier (ITB) in tokamaks and stellarators*. **(2)** Such results are based on ***four-time progress*** *in ion-confining potentials* (ϕ_c=3 kV) in comparison to ϕ_c attained 1992-2002 in association with the formation of a strong E_r shear. The data on ϕ_c well fit to a favorably increasing scaling with plug ECH powers. The advance in the potential formation leads to a finding of *remarkable effects of* $\mathbf{d}\boldsymbol{E_r}/\mathbf{d}\boldsymbol{r}$ on *turbulence suppression* and a *transverse-loss reduction*. **(3)** Under such physics understanding, the first *preliminary* central ECH (250 kW) raises T_{e0}=750 eV *(a new* ***five-time larger*** $\boldsymbol{T_e}$ ***record)*** together with $T_{i\perp 0}$=6.5 keV, and $T_{i//0}$=2.5 keV. On-axis energy drag (confinement) time from central-mirror trapped '$T_{i\perp}$' ions to electrons is significantly improved to be 0.14 s. On-axis energy confinement time for ϕ_c (=2.5 kV) confined '$T_{i//}$' ions reaches 0.16 s with 380-kW plug ECH applied for *both axial* E_z plugging and strong $\boldsymbol{E}_r\times\boldsymbol{B}$ sheared flow formation simultaneously. **(4)** *The* ***stored energy*** *of* ϕ_c ***potential confined ions*** between both plug regions ***exceeds*** *that (diamagnetism) of the central-cell* ***magnetically trapped ions*** for the first time. **(5)** A *weak decrease in* ϕ_c *with increasing* n_c ranging to $\sim 10^{19}$ m^{-3} along with the *recovery of* ϕ_c with *increasing plug ECH powers* is preferably obtained.

1. Introduction

Anomalous cross-field transport is one of the most critical issues in improvement of magnetized fusion plasma confinement. Some regimes with reduced anomalous transverse transport have been observed in tokamaks [1]. It is of essential importance for the progress in fusion programs to control the transition toward such regimes.

According to recent theories [1], transition to an H-mode with improved plasma confinement or the formation of internal transport barriers (ITB) in toroidal systems is associated with an increase in non-uniform radial electric fields E_r and a corresponding enhancement of sheared plasma rotation. Remarkably, the low-frequency plasma turbulence and the resultant anomalous transport observed in various devices exhibit rather common features [1-4].

Recently, intermittent turbulent vortex structures and effects of their suppression by strongly sheared plasma rotation were observed in the GAMMA 10 tandem mirror [2-4]. The suppression of turbulence and the associated significant reduction in cross-field transport in GAMMA 10 show behaviors that are similar to those seen for L-H transitions in tokamaks [2-5]. Mirror devices, having open-ended regions, provide intrinsic important advantages in terms of the control of radial-potential or sheared ***E***×***B*** rotation profiles on the basis of axial particle loss control for ambipolar potential formation [2-4].

In this paper, the effects of *actively controlled* radial potential or E_r shear flow profiles on the basis of *off-axis resonant* electron cyclotron heating (ECH) [3] are demonstrated. Formation of an alternative radial transport barrier, which has similar properties to ITB in toroidal plasmas [1], has been observed in the vicinity of the strong shear flow layer with a high vorticity. Decoupling and reduction of intermittent turbulent structures across the transport barrier region are found with temperature rises in the core plasmas. *This new method for an active control of the formation of radial energy transport barrier* is visually highlighted by the suppression of intermittent broadband fluctuations or vortex-like structures in L-mode like turbulent plasmas, which are produced by ion cyclotron heating (ICH) with ion temperatures $T_{\mathrm{i}} \sim 4$ keV for the off-axis ECH target.

On the basis of the physics understanding of E_{r} shear importance, *preliminary* central ECH (250 kW) is applied in a standard tandem-mirror operation with 380-kW plug ECH, which plays an essential role in ***both*** E_{z} plugging for an ***axial*** confinement improvement *and* automatically associated strong E_r shear flow for a ***radial*** confinement improvement *simultaneously*. The results of a significant rise in $T_{\mathrm{e}0}$ from 70 eV to 750 eV together with $T_{\mathrm{i}\perp 0}$=6.5 keV, and $T_{\mathrm{i}//0}$=2.5 keV is reported in Sec. 5. ***Both*** on-axis energy drag (confinement) time from central-mirror trapped ions to electrons (significantly improved to be 0.14 s), *and* on-axis energy confinement time for ϕ_{c} confined ions (reaching 0.16 s) are presented.

The plasma parameter improvements provide the following *first achievement* (Sec. 5). The ***stored energy*** *of* ϕ_c ***potential confined ions*** between both plug regions ***exceeds*** *that (**diamagnetism**) of the central-cell mirror* ***magnetically trapped ions*** for the first time.

2. Experimental Apparatus

GAMMA 10 [2-4,6,7], which is a minimum-B anchored tandem mirror with outboard axisymmetric plug and barrier cells, has an axial length (L_z) of 27 m, and the vacuum vessel of 150 m^3. In the central cell (L_z=6 m, limiter diameter =36 cm, and magnetic fields B_z=B_{m} at the midplane of 0.405 T, with a mirror ratio R_{m} of 5.2.). Ion cyclotron heating (30 kW at 6.36 MHz for central-cell hot-ion production, and 30 kW at 9.9 or 10.3 MHz for anchor-cell stabilization) is applied. The plug and barrier cells are axisymmetric mirrors with L_z=2.5 m, B_{m}=0.497 T, and R_{m}=6.2 for standard operations. In the transport barrier experiments, 4.75% higher B_{m} (0.519 T) is applied in the barrier cell for the off-axis resonant ECH to produce the cylindrical energetic electron layer. Gyrotron power of 120 kW at 28 GHz is injected into a single (east) barrier cell alone. No additional ECH is applied, thereby simplifying the experimental situations for electron transport analyses (see Sec. 4).

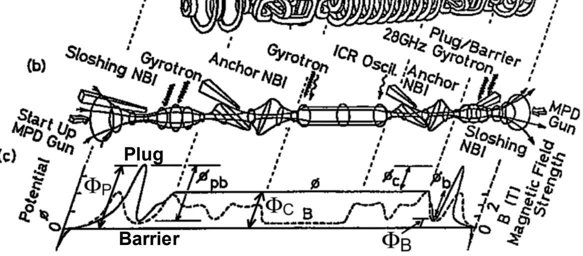

FIG. 1. Schematic view of the GAMMA 10 tandem mirror; (a) magnetic coil set, (b) magnetic flux tube with heating systems, as well as (c) axial magnetic field (dashed curve) and potential profiles (solid curve).

Various fluctuation diagnostics, which include a movable microwave interferometer, the Fraunhofer-diffraction method, two sets of our developed fifty-channel soft X-ray tomography detectors using microchannel plates (MCP)

[2-4] in the central-cell midplane, several original semiconductor detectors in various cells for T_e and T_i diagnostics [2-4], eight Langmuir probes for wave phasing and coherence diagnostics, heavy-ion (Au^0) beam probes (HIBP) and eight sets of ion-energy-spectrometer (IES) arrays [2-4], and simultaneous potential diagnostics with HIBP and IES show consistent characteristics (see below). Energetic electron currents are observed with a radially movable conventional end-loss analyzer (ELA) and ELA arrays at the west end.

Plug potentials Φ_P are measured with originally developed electrostatic spectrometer arrays, IES, for end-loss-ion energy analyses. Central-cell potentials Φ_C and barrier potentials Φ_B are directly measured with heavy-ion (Au^0) beam probes (HIBP). Therefore, one can obtain ϕ_c and ϕ_b, as Φ_P-Φ_C and Φ_C-Φ_B, respectively.

3. Four-Times Progress in the Formation of Ion-Confining Potentials ϕ_c as Compared to ϕ_c Attained 1992-2002

Four-time progress in ion-confining potentials ϕ_c to 3.0 kV in comparison to ϕ_c attained 1992-2002 is achieved in the hot-ion mode (T_i = several keV) (Fig. 2).

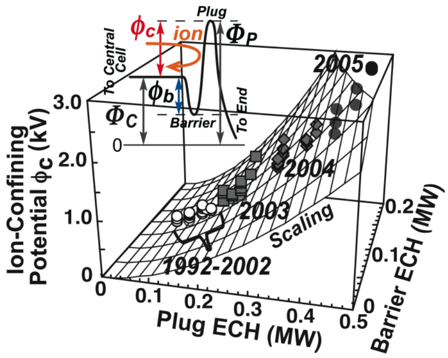

FIG. 2. Four-time progress in ϕ_c for confining central-cell ions (filled symbols) [see ϕ_c during 1992-2002 (open circles)] in accordance with a favorably rising scaling surface of plug and barrier ECH powers. T_i=several keV (the hot-ion mode).

As reported in [2-5], central-cell X-ray data show spatially and temporally fluctuated *vortex*-like structures during a *weakly sheared* period with 4 keV ICH plasmas. These "L-mode-like" turbulent structures, however, *clear up* with plug ECH, which produces a strong shear *over* plasma radii r_c. This results in a significant reduction of radial transport because of destroying turbulent "radial-transport shortcuts".

For the suppression of turbulence, we reported the usefulness of higher plug potentials Φ_P or ϕ_c formation *over all* r_c [2,4], since a strong central-cell dE_r/dr_c is proportional to the on-axis central-cell potential Φ_{C0}, and Φ_{C0} is raised by a Φ_P rise due to transit electrons between the central-cell and plug regions; i.e., $dE_r/dr_c = -d^2/dr_c^2(\Phi_{C0}\exp[-(r_c/a)^2]) = 2(1/a)^2[1-2(r_c/a)^2] \times(\Phi_{C0}\exp[-(r_c/a)^2])$; generally, $W \propto \Phi_{C0}$ [2,4,5].

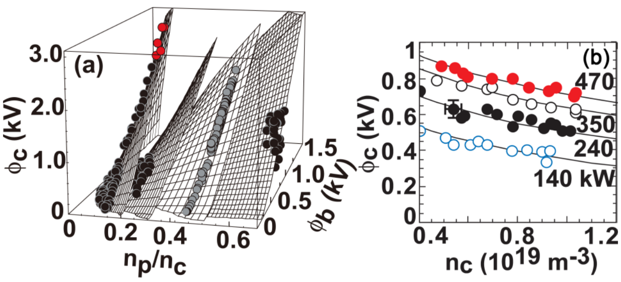

FIG. 3. Scalings of ion-confining potential ϕ_c formation for central-cell ions in (a) various parameters [4,7], and (b) as a function of plug ECH powers and central-cell densities n_c.

For *physics interpretations of ϕ_c formation*, the validity of our proposed mechanisms [4,7] is verified under various plasma parameters [Fig. 3(a)]. This encourages the future extendable scalability of the ϕ_c formation mechanism.

The scaling of ϕ_c [4] with n_c and P_{PECH} is investigated in Fig. 3(b). A *weak decrease in ϕ_c* with increasing n_c ranging to ~10^{19} m^{-3} is obtained along with the *recovery of ϕ_c with increasing* P_{PECH} [Fig. 3(b)]. These scalings in Fig. 3 encourage the control scenario of potentials, which contributes to both E_z axial (z) plugging and E_r sheared radial (r_c) confinement improvement.

4. Active Control of Transverse Energy-Transport Barrier Formation Due to the Formation of a Localized Sheared E×B Flow

From the viewpoint of the mechanism investigation of radially *localized* transport-barrier formation with relation to toroidal devices, an idea of *off-axis-resonant* (*barrier*) *ECH* is proposed and applied [Fig. 4] by the use of the aforementioned *intrinsic advantage* in potential formation of *open-ended mirror* devices. This allows to make flexible experiments for finding relations between shear profiles and reduction in turbulence-driven radial losses *due to ECH power-profile control*. Indeed, illustrated cross-section of the cylindrical layer [Fig. 5(b)] with energetic electrons [≈2 keV and *merely* small (≈10^{-5}) population to the total n_c in the layer] is observed. No beta-value effects and negligible slowing down plasma heatings are anticipated from the parameters. The cylindrical layer is centered near r_c=5.5 cm with its half width ≈1.5 cm, and formed along the whole device [Fig. 4] due to the *off-axis ECH* (t >149.2 ms). As described above, the loss of the energetic electrons leads to create a positively bumped potential enhancement located in the cylindrical layer with E_r shear formation.

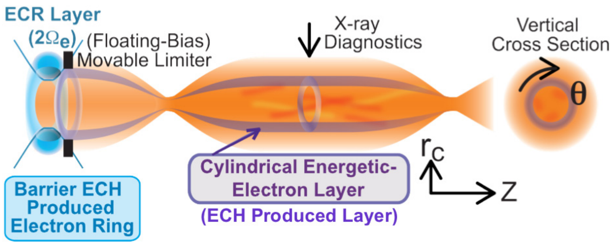

FIG. 4. Experimental configuration for radial transport barrier formation by the use of off-axis barrier ECH.

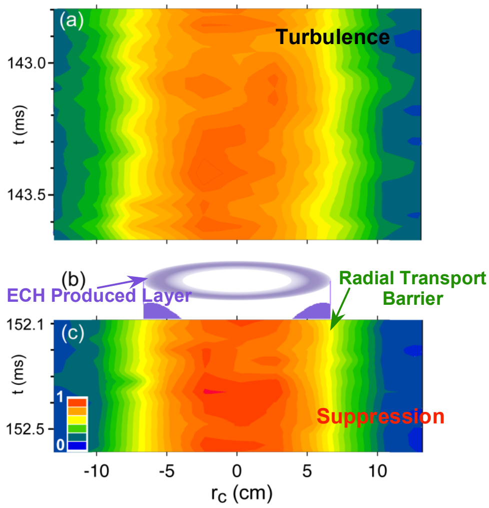

FIG. 5. Contours of central-cell X-ray brightness (a) with and (c) without cylindrically shaped energetic electron layer formation in (b) due to off-axis barrier ECH [see Fig. 4]. Hot-colored areas show higher plasma pressure locations. Strong turbulence with vortex-like structures continues to exist at r_c<4 cm in (a) and (c). However, its quietly suppressed region in (c) is observed in the energetic-electron layer [5<r_c<7 cm] and the outer surrounding cylindrical layer (7≤r_c<10 cm). ($I \propto n_e n_i T_e^{2.3}$.)

To investigate the effects of the energetic electron layer on the behavior and structure of turbulent plasmas [Fig. 5(a)], the contours of the central-cell soft X-ray brightness I_{sx} are shown [see Figs. 5(a) and (c) before and during ECH, respectively]. The internal regions (r_c<4 cm) indicate higher plasma pressure location. Spatially and temporally varied intermittent turbulent vortex-like structures in the internal region are evident in Figs. 5(a) and (c); whereas, the layer formation reduces the turbulence in the layer and the outer region (7≤r_c<10 cm) [Fig. 5(c)], where small temporal variations of the contours are found.

Fourier amplitudes of X-rays at r_c=2.7 and 10 cm without and with the layer formation (around t=146.5, and 152.5 ms) are shown in Figs. 6(a)-(d), respectively. Similarly, those from the IES array at r_c=2.6 [Figs. 6(e) and (f)] and 8.3 cm [Figs. 6(g) and (h)] in the absence [Figs. 6(e) and (g)] and presence [Figs. 6(f) and (h)] of the layer are presented. Turbulent spectra at any r_c without the layer [Figs. 6(a), (c), (e), and (g)], and the core region inside the layer [Figs. 6(b) and (f)] are similarly observed for both X-ray and ion signals. On the other hand, the turbulence is significantly reduced with the layer formation [Figs. 6(d) and (h)].

The frequency-integrated amplitudes over the broadband turbulent fluctuations from the X-ray and IES array detectors at various radii are summarized in Figs. 6(i) and (j), respectively. The filled and open circles in Figs. 6(i) and (j) correspond to the situation with and without the layer formation, respectively. In both figures, it is clear that a significant reduction in turbulent fluctuations is attained in and outside the layer ($5<r_c<10$ cm). These behaviors are consistently observed for visualized signals in Fig. 5.

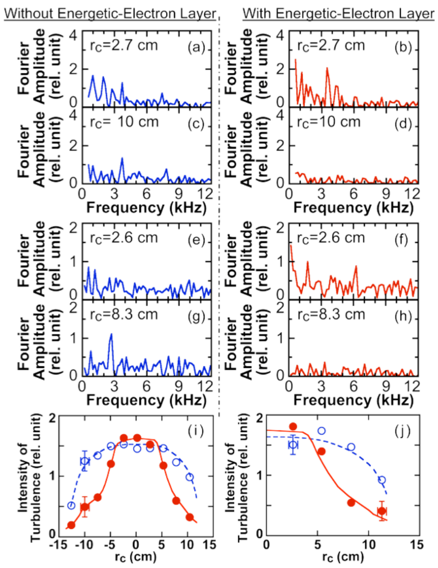

FIG. 6. Fourier amplitudes of (a)-(d) the central-cell X-ray signals in Fig. 5 and (e)-(h) those of ions with IES arrays are plotted at various r_c. The data sets are obtained in the absence [(a), (c), (e), (g)] and presence [(b), (d), (f), (h)] of the cylindrical energetic electron layer [Fig. 5(b)]. Frequency integrated amplitudes over the broadband turbulent fluctuations in the X-ray and IES array data are summarized in (i) and (j), respectively. The filled and open circles show the cases with and without the layer, respectively. A significant reduction of the turbulence is attained in the layer and outside the layer ($5<r_c<10$ cm). These behaviors are consistent with those in Fig. 5.

In Fig. 7(a), the solid and dashed curves show Φ_C profiles in the presence and absence of the layer formation, respectively (see also the inserted shaded region for the electron current density profile [$4<r_c<7$ cm] observed with the radially movable ELA). In the presence and absence of the layer, radial profile data from the central-cell HIBP and (west) IES arrays [2-4] are plotted with the filled and open circles, respectively. Loss of the produced energetic electrons flowing into end regions leads to form a bump of the ambipolar potential Φ_C.

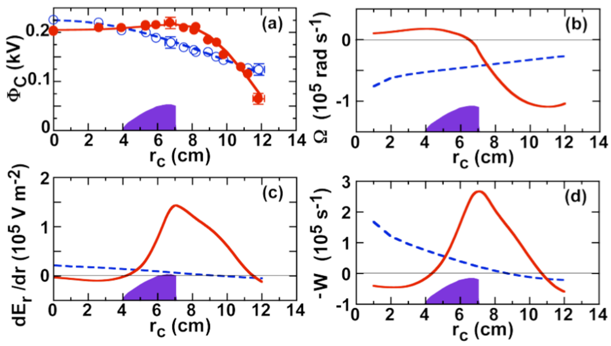

FIG. 7. (a) Central-cell potential data from HIBP and IES arrays are plotted with the filled and open circles, respectively, along with the solid and dashed fitting curves for the presence and absence of the energetic-electron layer, respectively. The inserted shaded region shows the observed profile of the electron-current density [$4<r_c<7$ cm]. (b) The angular velocity having direction reversal of the E_r×B azimuthal drift flow across the bumped locations of (c) E_r shear and (d) dynamic vorticity at $r_c\approx 7$ cm is plotted in the presence of the energetic-electron layer (the solid curves). A significant reduction of the turbulent fluctuations ($5<r_c<10$ cm), and a high level of fluctuations in the core plasma at $r_c<4$ cm (Figs. 5 and 6) are observed. ($n_e=1.6\times10^{18}$ m^{-3} at $r_c=6$ cm.)

Such a bumped profile of Φ_C results in changes of the signs of the gradient Φ_C and E_r at the Φ_C peaked location, $r_c\approx 7$ cm$\equiv r_p$. This means the *direction reversal* of the $\boldsymbol{E}_r\times\boldsymbol{B}$ azimuthal (θ) drift flow across $r_c=r_p$; that is, the oppositely directed $\boldsymbol{E}_r\times\boldsymbol{B}$ sheared drift flows separate plasmas into two regions at $r_c=r_p$ from the viewpoint of actual plasma motions in θ. This feature of the angular velocity (Ω) reversal from positive to negative values across $r_c=r_p$ is shown by the solid curve in Fig. 7(b).

Further essential features can be seen in the behaviors of the radial plots of the E_r shear [Fig. 7(c)] and the dynamic vorticity W [Fig. 7(d)]. As shown in [5], W plays a role in the canonical momentum of rotational motion in magnetized plasmas with non-uniform density. It provides a natural generalization of the vorticity vector $\boldsymbol{w}=\nabla\times\boldsymbol{V}$, which is well-known as a canonical momentum and a measure of velocity shear in the dynamics of incompressible fluids. The z-component of the normalized dynamic vorticity $W=[\nabla\times(n\boldsymbol{V}_E)]_z/n_0=d/dr_c[nr_c^2\Omega]/(n_0 r_c)$ (where n_0 is the on-axis density) is chosen to characterize $\boldsymbol{E}\times\boldsymbol{B}$ velocity ($\boldsymbol{V}_E$) shear in our experiments [2-4]. In the presence of the layer, the Φ_C bump in Fig. 7(a), which leads to a rapid change in Ω [Fig. 7(b)], provides significant bumps in the dE_r/dr_c and W profiles [Figs. 7(c) and (d)], respectively. A large-valued regime in W with the bump, centered near r_c=7 cm, cover the radii with the significant reduction in the turbulence fluctuations ($5<r_c<10$ cm). On the other hand, a high level of fluctuations in the core plasma corresponds to the weakly sheared small W regime at $r_c<4$ cm.

Comparisons of the T_e and T_i profiles are shown in Figs. 8(a) and (b), respectively, from the X-ray and charge-exchanged particle analyses. One can confirm steep gradients for both T_e and T_i in this large W regime along with the resulting higher T_e and T_i in the core region surrounded by this steep gradient layer having a strong shear [Figs. 7(c) and (d)]. These findings of radially improved T_e and T_i profiles surrounded by the localized shear flow layer allow us to collaborate analogical similarity studies of radial transport-barrier formation in toroidal devices [1]. For instance, local heating on a magnetic surface (with some radial local losses) is a candidate for actively producing similar ambipolar-potential bump and barrier.

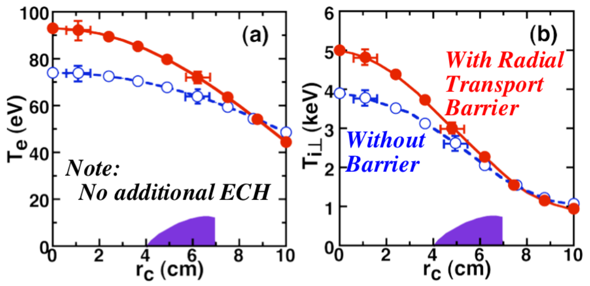

FIG. 8. The solid and dashed curves show (a) T_e and (b) T_i profiles from X-ray and charge-exchanged particle analyses in the presence and absence of the energetic electron layer (illustrated shaded regions), respectively. Steep gradients in both T_e and T_i in a large W_r regime along with rather flat and higher T_e and T_i in the inner region surrounded by the layer are found. For simplicity, neither plug nor central ECH is injected.

These results allow us to interpret that large-scaled turbulence typically exists in a standard regime that has a radially smooth profile of a weakly sheared plasma rotation. Stochastic vortex structures with characteristic scales comparable with the plasma radius, dominate the turbulence and causes enhanced radial heat transport. Experimental results show that the presence of a high W layer leads to suppress turbulent fluctuations, and forms steep T_e and T_i gradients across the layer [Fig. 8]. Furthermore, the large-scaled vortices localized in the plasma core and turbulence at the plasma edge (e.g. the probe diagnostics) appear to be independent of each other. This decoupling of dominant structures is an alternative example of reduction of the radial correlation length due to sheared flows.

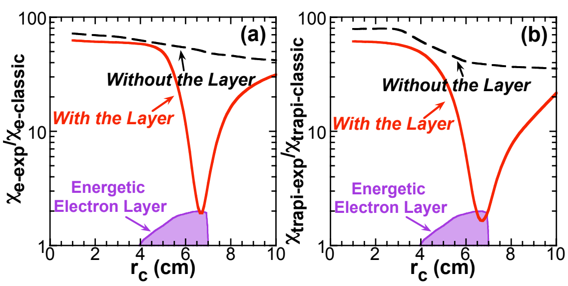

FIG. 9. For reference, thermal diffusivities of central-cell mirror trapped ions and electrons are compared with those calculated from classical (Coulomb collision transport) theories in the case with energetic electron layer formation due to the off-axis barrier ECH application. In the high vorticity [strong E_r shear] region, significant suppression of transverse ion and electron losses is indeed identified (see the solid curves).

In Fig. 8(a), T_e rises in the core region due to reduction of the effective radial thermal diffusivity $\chi_{e\perp}$ in the high W layer to the classical value of 3×10^{-3} m^2 s^{-1} at these plasmas together with axial plugging by floated endplate potential depth ($\approx3T_e$) [6] [Fig. 9(a)]. Furthermore, enhancement of T_i for central-mirror confined ions [Fig. 8(b)] is well interpreted by the absence of appreciable anomalous ion radial losses across the layer and by the classical electron drag (see the small diffusivity $\chi_{i\perp}$ [Fig. 9(b)] in the high W layer). Continuity of total transverse fluxes necessarily leads to the local enhancement of temperature gradients [Fig. 8]. Indeed, the T_e gradient becomes steeper by a factor of two in the high W region ($5<r_c<10$ cm), while the temperature profiles in the weakly sheared plasma core remain rather flat. Following the conventional definition of ***ITB*** [1], we interpret these effects as alternative *formation of an internal transport barrier* in the area that has an actively controlled high-velocity shear.

5. Improvements in Plasma Parameters

On the basis of the physics understanding of the importance of E_r sheared flow, *preliminary* central-cell ECH (250 kW) is applied in a standard tandem mirror operation with 380 kW plug ECH, which plays an essential role in ***both*** E_z plugging for an ***axial*** confinement improvement *and* the automatically associated strong E_r shear flow for a ***radial*** confinement improvement simultaneously. As a result, a significant rise in T_{e0} from 70 eV to 750 eV [Fig. 10(a)] together with $T_{i\perp0}$=6.5 keV for central mirror trapped ions, $T_{i//0}$=2.5 keV for ϕ_c (=2.5 kV) confined ions, and ϕ_b=0.93 kV is stably obtained with launched 86 kW ICH (absorbed η_{ICH}=0.37 for $nl_c=4.5\times10^{17}$ m^{-2}). *The* ***on-axis energy drag (confinement) time*** $\boldsymbol{\tau_{E0}}$ from the *central* ***mirror trapped ions*** to electrons is significantly improved to be 0.14 s ($\approx$ the simple mirror confinement time for the 6.5 keV ions), *and the* ***on-axis energy confinement time*** $\boldsymbol{\tau_{E0}}$ for ϕ_c ***potential confined*** *2.5 keV* ***ions*** reaches 0.16 s. In comparison to radially averaged energy confinement time [=(stored energy) / (absorbed ion heating power)], ***local*** $\boldsymbol{\tau_E(r_c)}$ ***values*** are ***integrated and averaged*** *over* r_c, since $\phi_c(r_c)$ has a similar radial profile to the plug ECH power-lobe (the Gaussian) shape. In the present case with the ECH Gaussian profile lobe, the ratio of the *radially averaged global energy confinement time* $<\tau_E>$ to the *on-axis value* τ_{E0} ranges 0.52-0.45 because of the inclusion of smaller confinement times in the lower potential and weakly sheared outer (larger r_c) regions *for* $<\tau_E>$ (e.g. in the above-described case, ***radially averaged*** $<\tau_E>$ ranges 72 ms). Here, for estimating the **stored energy** ***including*** significantly rising parameters $d(3/2n_iT_i)/dt$ of the magnetically and potentially confined ions, we take account of the volume difference of 0.3 between the central-cell mirror plasmas and the plug-to-plug ϕ_c confined plasmas (see Fig. 1) along with nearly the same density ratio observed for the magnetically and potentially confined ions. The radially averaged $<\tau_E>$ is consistent with a roughly estimated value of [(stored energy) / (absorbed ion heating power)]. If employed a broader plug ECH lobe, one would obtain radially averaged larger stored energy and longer global confinement time $<\tau_E>$.

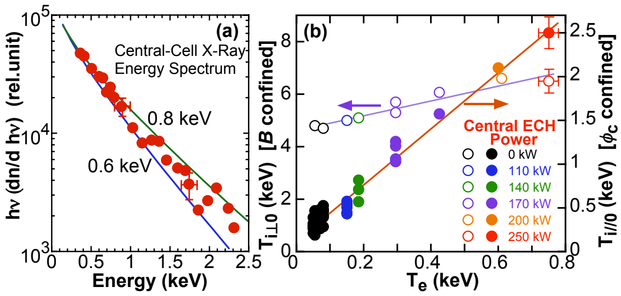

FIG. 10. (a) Direct heating due to central-cell ECH raises T_e over 0.7 keV (i.e. X-ray PHA). (T_{e0}=0.75 keV from X-ray tomography). (b) Reduction of electron drag for central-cell ions highlights that the stored energy of ϕ_c potential confined ions between both plugs exceeds that (diamagnetism) of central-cell magnetically mirror trapped ions.

In consequence of these plasma parameter improvements, it is highlighted that the ***stored energy*** *of* ϕ_c ***potential confined ions*** between both plug regions, which characterize tandem mirror potential confinement, has ***exceeded*** the stored energy *(****diamagnetism****)* of *central-cell* *mirror* ***magnetically confined ions*** [Fig. 10(b)] for the first time through the tandem mirror history due to a significant increase in T_e (i.e. the ion pitch-angle scattering time from "$T_{i\perp}$ into $T_{i//}$" approaching comparable to the electron drag time for the mirror trapped ions with "$T_{i\perp}$").

6. Summary

(1) A ***transverse energy-transport barrier*** is *produced* and ***externally controlled*** for the first time (Figs. 4-9) by *off-axis ECH* (Fig. 4) at $4<r_c<7$ cm [3]. In this region, a radially localized *ambipolar-potential bump* with *strongly sheared electric fields* E_r is formed (Fig. 7).

(2) Both $\boldsymbol{T_e}$ **and** $\boldsymbol{T_i}$ **increase** in the core plasma region, surrounded by this strong shear flow layer (Fig. 8). The rises are associated with the *suppression of L-mode-like intermittent turbulent vortex-like structures* (Fig. 5). The effective radial thermal diffusivity $\chi_{e\perp}$ as well as $\chi_{i\perp}$ in the sheared layer approach to the classical values (Fig. 9). These behaviors are similar to those of *internal transport barrier (**ITB**) formation in tokamaks and stellarators* [1].

(3) Such results are based on ***four-time progress*** *in ion-confining potential height* (ϕ_c=3 kV) in comparison to ϕ_c attained 1992-2002 (Fig. 2) in association with the formation of a strong E_r shear. The ϕ_c data well fit to a favorably increasing scaling with plug ECH powers, P_{PECH}.

(4) *Preliminary* **central-cell ECH** (250 kW) raises T_{e0}=750 eV (***five-time larger*** $\boldsymbol{T_e}$ ***record***) together with $T_{i\perp 0}$=6.5 keV, and $T_{i//0}$=2.5 keV. The on-axis energy drag (confinement) time τ_{E0} from central-cell mirror trapped "$T_{i\perp}$" ions to electrons is significantly improved to be 0.14 s together with τ_{E0} for ϕ_c confined "$T_{i//}$" ions reaches 0.16 s with 380-kW plug ECH.

(5) The ***stored energy*** *of* ϕ_c ***potential confined ions*** between both plug regions, characterizing tandem-mirror potential confinement, has ***exceeded*** the stored energy (**diamagnetism**) of central-cell mirror ***magnetically confined ions*** [Fig. 10(b)] for the first time.

(6) For the scaling of ϕ_c [4] with n_c and P_{PECH}, a *weak decrease in* ϕ_c with increasing n_c ranging to ~10^{19} m^{-3} is obtained along with the *recovery of* ϕ_c *with increasing* P_{PECH} [Fig. 3(b)]. These scalings in Fig. 3 encourage the control scenario of potentials, which contributes to ***both*** E_z axial (z) plugging for an ***axial*** confinement improvement *and* the automatically associated strong $\boldsymbol{E_r \times B}$ shear flow for a ***radial*** confinement improvement simultaneously.

**Permanent Address*;
[1] Art, Science and Technology Center for Cooperative Research, Kyushu University, Japan
[2] Department of Electrical and Electronics Engineering, Kobe University, Japan
[3] Japan Atomic Energy Agency, Naka, Ibaraki, Japan
[4] Institute for Fusion Studies, University of Texas at Austin, USA
[5] Russian Research Center "Kurchatov Institute", Moscow, Russia

[1] DIAMOND, P. H., et al., Plasma Phys. Control. Fusion **47** (2005) R35; KISHIMOTO, Y., et al., Nucl. Fusion **40** (2000) 667.
[2] CHO, T., et al., Phys. Rev. Lett. **94** (2005) 085002.
[3] CHO, T., et al., Phys. Rev. Lett. **97** (2006) 055001.
[4] CHO, T., et al., Nucl. Fusion **45** (2005) 1650; Fusion Energy 2004 (Proc. 20th Int. Conf. Vilamoura, 2004), IAEA, Vienna, CD-ROM file EX/9-6Rd; and http://www-naweb.iaea.org/napc/physics/fec/fec2004/datasets/index.html.
[5] PASTUKHOV, V. P., Plasma Phys. Reports **31** (2005) 577; JETP Lett. **82** (2005) 395.
[6] MIYOSHI, S., et al., Fiz. Plazmy **23** (1997) 781. (Plasma Phys. Rep. **23** (1997) 723.)
[7] CHO, T., et al., Phys. Rev. Lett. **86** (2001) 4310.